Voltage-Regulated Water Flux through Aquaporin Channels In Silico

Jochen S. Hub,[†△*] Camilo Aponte-Santamaría,[‡△] Helmut Grubmüller,[‡] and Bert L. de Groot[‡]
[†]Department for Cell and Molecular Biology, Uppsala University, Uppsala, Sweden; and [‡]Department of Theoretical and Computational Biophysics, Max-Planck-Institute for Biophysical Chemistry, Göttingen, Germany

ABSTRACT Aquaporins (AQPs) facilitate the passive flux of water across biological membranes in response to an osmotic pressure. A number of AQPs, for instance in plants and yeast, have been proposed to be regulated by phosphorylation, cation concentration, pH change, or membrane-mediated mechanical stress. Here we report an extensive set of molecular dynamics simulations of AQP1 and AQP4 subject to large membrane potentials in the range of ± 1.5 V, suggesting that AQPs may in addition be regulated by an electrostatic potential. As the regulatory mechanism we identified the relative population of two different states of the conserved arginine in the aromatic/arginine constriction region. A positive membrane potential was found to stabilize the arginine in an up-state, which allows rapid water flux, whereas a negative potential favors a down-state, which reduces the single-channel water permeability.

Received for publication 3 September 2010 and in final form 3 November 2010.

[△]Jochen S. Hub and Camilo Aponte-Santamaria contributed equally to this work.

*Correspondence: jochen@xray.bmc.uu.se

Aquaporins (AQPs) form a large family of protein channels that facilitate the passive permeation of water across biological membranes in response to osmotic pressure (1). Related aquaglyceroporins allow, in addition to water, the permeation of other small solutes such as ammonia, glycerol, and urea. AQPs are expressed in all domains of life and 13 different AQPs were so far discovered in humans, termed AQP0–AQP12 (2). More recently, the regulation of AQPs has emerged as an active field of research. Plant AQPs are gated by phosphorylation or alterations in pH and cation concentrations, whereas N- and C-terminal domains regulate Aqua(glycero)porins in yeast (3). In addition, trafficking of mammalian AQPs from intracellular storage vesicles to the plasma membrane, triggered by phosphorylation, has been shown to modulate membrane permeabilities (4).

The possibility of voltage-regulated AQPs has not been considered so far, possibly in part because no physiological function has thus far been related to voltage-regulation or because alterations in water permeability in response to voltage modulations may be difficult to assess experimentally. To test the hypothesis of potential voltage regulation in AQPs, we have employed full-atomistic molecular dynamics simulations to study water permeation through AQP1 and AQP4 as a function of an applied electrostatic membrane potential. To assess the effect of a membrane potential on the water flux, we have set up simulation systems of two AQP tetramers stacked on top of each other, and separated by two water compartments (Fig. 1 *A*). Because the simulations were carried out with periodic boundary conditions, the top and bottom of the simulation box in Fig. 1 *A* correspond to a single outer water compartment. Each tetramer was embedded in a lipid membrane, and 150 mM sodium chloride was added to each of the two water compartments. The membrane potential was subsequently generated by adding cations to the central compartment (*red* + in Fig. 1 *A*) and anions to the outer compartment (two *blue* – in Fig. 1 *A*). Consequently, the two AQP tetramers are subject to a membrane potential of opposite sign but identical magnitude, where the magnitude is controlled by the number of additional cations and anions in the central and outer compartments, respectively. More details on the simulation setup are provided in the Supporting Material.

Fig. 1 *B* presents the electrostatic potential $\Phi(z)$ as a function of coordinate z (membrane normal). Note that $\Phi(z)$ is plotted in accordance to the simulation box in Fig. 1 *A*, allowing one to identify the peaks in $\Phi(z)$ as the intramembrane potential, and the flat parts in $\Phi(z)$ as the potential between the compartments. The membrane potential $\Delta\Phi$ is thus given by the potential difference between the two water layers (*black arrow*). The different colored curves in Fig. 1 *B* correspond to AQP1 simulations of different membrane potentials. The simulated membrane potentials lie in the range of –1.5 to +1.5 V, one-order-of-magnitude larger than typical physiological potentials.

Fig. 2 *A* shows AQP1 single-channel water permeabilities p_f as a function of membrane potential, where each p_f value was derived from 60 ns of simulation. Remarkably, p_f is regulated by the membrane potential, with higher permeabilities at positive membrane potential, defined by a higher $\Phi(z)$ in the intracellular as compared to the extracellular side of AQP1 (*upper AQP1 tetramer* in Fig. 1 *A*). In contrast, we find smaller p_f values for a negative membrane potential (*lower AQP tetramer* in Fig. 1 *A*). Despite the substantial

Editor: Gerhard Hummer.

doi: 10.1016/j.bpj.2010.11.003

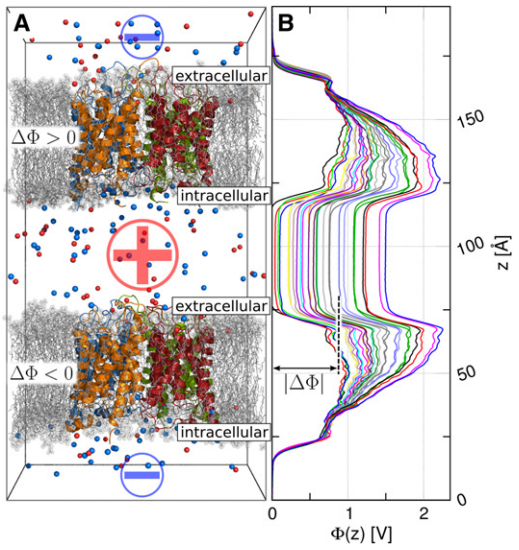

FIGURE 1 (*A*) Simulation box of two stacked aquaporin-1 tetramers (*cartoon representation*) embedded in a phospholipid membrane (*gray sticks*), and solvated in water (not shown) and 150 mM sodium chloride (*red* and *blue spheres*). The electrostatic membrane potential was generated by additional cations to the central compartment (*red* +) and additional anions to the outer compartment (two *blue* –). (*B*) Electrostatic potential $\Phi(z)$ along the membrane normal z during 25 simulations with increasing additional charges in the two water compartments. The membrane potential $\Delta\Phi$ is indicated by a black arrow.

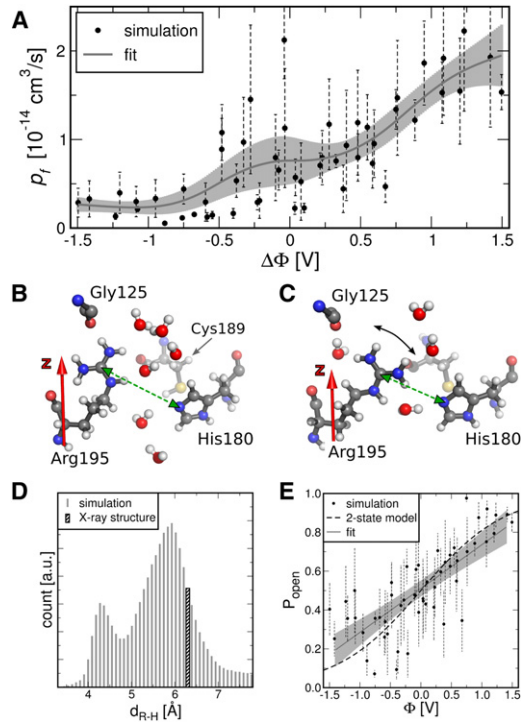

FIGURE 2 (*A*) Single-channel permeability p_f of AQP1 versus membrane potential $\Delta\Phi$. (*B* and *C*) Conserved Arg^{195} in AQP1 (*B*) in the up-state and (*C*) in the down-state. (*D*) Wide distribution of Arg^{195}-His^{180} distance $d_{R\text{-}H}$ taken from all simulations. $d_{R\text{-}H}$ in x-ray structure is indicated by a shaded bar (6). (*E*) Probability for an open channel versus $\Delta\Phi$. Linear fit (*shading*) and P_{open} derived from a two-state model (*dashed*).

simulation time used to compute the p_f values, the individual values scatter substantially (Fig. 2 *A*, *black dots*). Hence, p_f converges relatively slowly with simulation time, suggesting that the large number of simulations employed here is indeed required to yield a robust p_f versus $\Delta\Phi$ signal. To guide the eye, we have fitted a spline function to the data points in Fig. 2 *A* (*shaded curve*), where the shaded area indicates the statistical error of the fitted spline computed by bootstrap analysis (see the Supporting Material).

From visual inspection of the simulation trajectories, the conserved Arg^{195} in the aromatic/arginine region (ar/R) emerged as the putative voltage gate. In all simulations, Arg^{195} was flexible and frequently visited (at least) two conformational states, which differ in the dihedral angle along the C_γ-C_δ bond. Two frequently adopted states are visualized in Fig. 2, *B* and *C*, and in the following referred to as up- and down-states. In the up-state, Arg^{195} is stabilized by an intra-Arg^{195} hydrogen bond (H-bond) and by an H-bond to Gly^{125} of Loop-C (Fig. 2 *B*), allowing a continuous water file and rapid water flux. In the down-state, the ar/R region is partly closed, the water file is interrupted, and a leverlike motion of the Arg^{195} side chain is required to allow the passage of a water molecule (*solid arrow* in Fig. 2 *C*). For this study, the protein was described by the OPLS all-atom force field. The two Arg^{195} states were also visited in AQP1 simulations that we carried out using the GROMOS96 force field (not shown) and have been reported in simulations using the CHARMM27 force field (5). The up-state was found in the x-ray crystallographic structures of AQP1 and AQP4 (6,7), but structural studies suggested that both, the up- and the down-state can be adopted in *Escherichia coli* AQP-Z (8). In addition, an alternative Arg^{195} position was found in AQP1 from electron crystallographic studies (9), suggesting that different Arg^{195} states, including the up- and the down-states, may indeed be populated under physiological conditions.

To quantify the openness of the ar/R region, Fig. 2 *D* presents the distribution of the Arg^{195}-His^{180} distance $d_{R\text{-}H}$ as visited during all simulations, demonstrating that the ar/R region can adopt a wide range of openness. Here, $d_{R\text{-}H}$ was defined as the distance from the C_ζ atom of Arg^{195} to the closest heavy atom of His^{180} (*green arrows* in Fig. 2, *B* and *C*). We stress that the two maxima in $d_{R\text{-}H}$ do not correspond to the *up* and *down* states. As a measure for a permeating open channel, Fig. 2 *E* shows the probability P_{open} for an open channel versus $\Delta\Phi$, where an open channel was defined from $d_{R\text{-}H} > 5.7$ Å. P_{open} correlates positively with $\Delta\Phi$, suggesting that the membrane potential indeed regulates the openness of the ar/R region.

Which molecular mechanism accounts for the shift in the relative populations of the up- and down-state?

Direct electrostatic forces acting on Arg^{195} play an important role, because the positively charged guanidinium group moves by $\delta_z \sim 1.5$ Å in z direction between the two states. To estimate whether the Arg^{195} displacement is sufficient to tune P_{open}, let us assume a simple open/closed two-state model for Arg^{195}, affected by a homogeneous electric field across the membrane (see the Supporting Material for details). That model yields a P_{open} as indicated by the dashed curve in Fig. 2 *E*, in reasonable agreement with a fitted line to the data points (*shaded line*), suggesting that direct electrostatic interactions of Arg^{195} may indeed tune the open probability of the ar/R region by about the observed factor, given the membrane potentials applied here.

To assess whether the voltage sensitivity of the conserved arginine may be a general feature of AQPs, we have carried out analogous simulations of human AQP4, using the setup shown in Fig. 1 *A*. 13 simulations of at least 50 ns each were carried out, applying membrane potentials between –1.4 and +1.4V. Remarkably, the conserved arginine (Arg^{216} in AQP4) again adopted two distinct up- and down-states, which are in this case clearly characterized from the $d_{R\text{-}H}$ distribution, taken from the 104 AQP4 monomers in the 13 simulations (Fig. 3 *A*). In the up-state, the channel is open at the ar/R region. Accordingly, $d_{R\text{-}H}$ in the crystal structure is at this region of the distribution (*shaded bar*). In contrast, in the down-state, the conserved Arg^{216} occludes the pore and prevents water passage. The up-state was predominantly visited when AQP4 was at positive membrane potentials (*upper tetramer* in Fig. 1 *A*), and the down-state at negative potentials (*lower tetramer* in Fig. 1 *A*). To further quantify how voltage shifts the distribution toward either of the two states, the probability P_{open} for an open ar/R region ($d_{R\text{-}H} > 5.7$ Å) was computed (Fig. 3 *B*). P_{open} correlates with $\Delta\Phi$, with the lowest P_{open} for negative $\Delta\Phi$, indicating a closed channel. A two-state model again agrees favorably with the data points, suggesting that the displacement of Arg^{216} is sufficient to explain P_{open}.

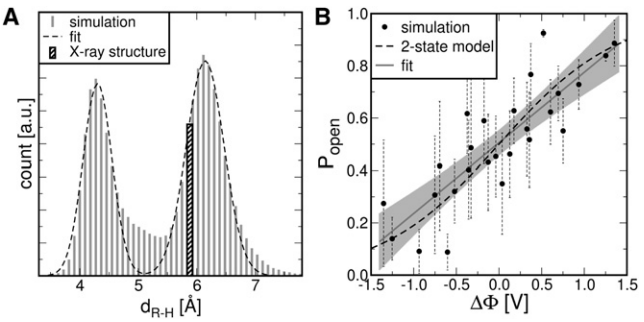

FIGURE 3 Voltage-sensitive openness of the aromatic/arginine (ar/R) region of aquaporin-4 (AQP4), as measured from the distance $d_{R\text{-}H}$ between Arg^{216} and His^{201}. (*A*) Distribution of $d_{R\text{-}H}$, taken from 13 AQP4 simulations at membrane voltages between –1.4 and +1.4 V (*shaded histogram*), revealing two distinct states. $d_{R\text{-}H}$ in the AQP4 crystal structure (7) is indicated by a shaded bar. (*B*) Probability for an open channel P_{open} versus $\Delta\Phi$. Linear fit (*gray*) and P_{open} derived from a two-state model (*dashed*).

Finally, we have carried out simulations in which AQP1 and AQP4 were restrained in the open or closed state (see the Supporting Material for details). The simulations confirm that the arginine position strongly regulates the water flux, suggesting that the tuning of P_{open} consequently also tunes p_f.

To conclude, we observed voltage-regulated singe-channel water permeabilities p_f of AQPs in molecular dynamics simulations, with a p_f decrease when switching from a positive to a negative membrane potential. Note that the potentials applied here are one order of magnitude larger than typical physiological potentials, with the simulations indicating only a moderate, yet measurable effect for physiological voltage ranges. We attribute the p_f regulation to a shift in the relative population of the up-state versus the down-state of the conserved arginine in the ar/R region, due to an applied electric potential. It will be highly interesting to test the simulation-based voltage regulation hypothesis in AQPs experimentally by measurements of the voltage-dependent water permeability. The effect may be measured using biological membranes, or, if large potentials are necessary to measure the effect, more robust artificial systems may be required.

SUPPORTING MATERIAL

One equation, one figure, and Materials and Methods are available at http://www.biophysj.org/biophysj/supplemental/S0006-3495(10)01370-6.

ACKNOWLEDGMENTS

We thank Peter Pohl for stimulating discussions.

This study was supported by the Marie Curie Research Training Network Aqua(glycero)porins (MRTN-CT-2006-035995) and by a Marie Curie Intra-European fellowship.

REFERENCES and FOOTNOTES

1. Preston, G. M., T. P. Carroll, …, P. Agre. 1992. Appearance of water channels in *Xenopus* oocytes expressing red cell CHIP28 protein. *Science.* 256:385–387.
2. King, L. S., D. Kozono, and P. Agre. 2004. From structure to disease: the evolving tale of aquaporin biology. *Nat. Rev. Mol. Cell Biol.* 5:687–698.
3. Törnroth-Horsefield, S., K. Hedfalk, …, R. Neutze. 2010. Structural insights into eukaryotic aquaporin regulation. *FEBS Lett.* 584:2580–2588.
4. Nedvetsky, P. I., G. Tamma, …, E. Klussmann. 2009. Regulation of aquaporin-2 trafficking. *Handb. Exp. Pharmacol.* 190:133–157.
5. Wang, Y., K. Schulten, and E. Tajkhorshid. 2005. What makes an aquaporin a glycerol channel? A comparative study of AqpZ and GlpF. *Structure.* 13:1107–1118.
6. Sui, H., B.-G. Han, …, B. K. Jap. 2001. Structural basis of water-specific transport through the AQP1 water channel. *Nature.* 414:872–878.
7. Ho, J. D., R. Yeh, …, R. M. Stroud. 2009. Crystal structure of human aquaporin 4 at 1.8 Å and its mechanism of conductance. *Proc. Natl. Acad. Sci. USA.* 106:7437–7442.
8. Jiang, J., B. V. Daniels, and D. Fu. 2006. Crystal structure of aquaporin Z tetramer reveals two distinct Arg-189 conformations associated with water permeation through the narrowest constriction of the water-conducting channel. *J. Biol. Chem.* 281:454–460.
9. Murata, K., K. Mitsuoka, …, Y. Fujiyoshi. 2000. Structural determinants of water permeation through aquaporin-1. *Nature.* 407:599–605.